Article

Positive Impact of Red Soil on Albedo and the Annual Yield of Bifacial Photovoltaic Systems in Ghana [†]

Eva-Maria Grommes [1,]*[], **Ulf Blieske** [1][] and **Jean-Régis Hadji-Minaglou** [2][]

1   Cologne Institute for Renewable Energy, University of Applied Sciences Cologne, 50679 Cologne, Germany
2   Department of Engineering, University of Luxembourg, 1359 Luxembourg, Luxembourg
*   Correspondence: eva-maria.grommes@th-koeln.de
†   This paper is an extended version of our paper published in 2022, Performance Estimation of Bifacial PV Systems Using the View Factor Matrix. 10.57683/EPUB-1991.

Abstract: The annual yield of bifacial photovoltaic systems is highly dependent on the albedo of the underlying soil. There are currently no published data about the albedo of red soil in western Africa. In this study, the impact of the albedo of red soil in Ghana on the energy yield of bifacial photovoltaic systems is analysed. A bifacial photovoltaic simulation model is created by combining the optical view factor matrix with an electrical output simulation. For an exact simulation, the albedo of red soil at three different locations in Ghana is measured for the first time. The average albedo of every red soil is clearly determined, as well as the measurement span including instrumentation uncertainty; values between 0.175 and 0.335 were measured. Considering these data, a state-of-the-art bifacial photovoltaic system with an average of 19.8% efficient modules in northern Ghana can achieve an annual energy yield of 508.8 kWh/m^2 and a bifacial gain of up to 18.3% in comparison with monofacial photovoltaic panels. To summarise, red soil in two out of three locations in Ghana shows higher albedo values than most natural ground surfaces and therefore positively impacts the annual yield of bifacial photovoltaic systems.

Keywords: solar energy; photovoltaic systems; bifacial photovoltaic; power system simulation; renewable energy simulation; red soil; Ghana; albedo

1. Introduction

The rising demand for energy and the low number of suitable areas for clean energy production demand more efficient energy technologies, such as bifacial photovoltaic (PV) systems [1]. These solar modules can absorb irradiance from the front and rear sides, resulting in a higher annual energy yield per module area than their monofacial counterparts and an enhancement of up to 35% in energy density [2]. An upward trend for the share of bifacial PV modules in the global market, from 28% to 55%, is predicted by the International Technology Roadmap for Photovoltaic (ITRPV) for the next decade [3]. This forecast is underlined by the latest growing trend in the world share of bifacial PV compared with monofacial PV modules.

Desert regions are of particular interest for the application of bifacial PV systems. In 2021, a 10 MW bifacial PV system on red soil in South Africa went online [4]. Even without current bifacial projects planned in Ghana, the country is considered to be comparable to South Africa, with similar global irradiation values of 4.5–6.5 kWh/m^2 per day [5] and the presence of red soil in large undeveloped areas. Therefore, Ghana is also considered a relevant country for bifacial performance research.

In a closer examination of the areas where bifacial PV systems can be installed, in West, East, and South Africa, red soil is the usual subsurface [6]. Due to the recurrent energy deficit in the country and the expected growth of both monofacial and bifacial PV technology, in this study, Ghana is taken as an exemplary country for the study of possible

red soil impacts on bifacial PV systems [7]. Considering a similar composition of red soil, the results are transferable to any other country with red soil.

Simulating bifacial PV adds more parameters to the estimation of energy yield, such as the ground-reflected irradiance on the rear side depending on the albedo. The view factor model of the existing bifacial radiance is complemented in order to calculate the resulting energy yield in the simulation. The simulation model calculating the impact of albedo on the energy yield of bifacial PV systems is validated by measurements [8,9]. It is expected that the albedo of red soil positively impacts the annual yield of bifacial PV systems.

2. Methodology

The conducted analysis investigates the impact of the albedo of red soil on the energy yield of bifacial modules in Ghana. The radiation reaching the front and rear sides of the bifacial PV module is calculated using the mathematical hybrid Perez model [10] for irradiance reflection and calculation of the diffuse light, and the 2D view factor model [11] for the radiance distribution. The presented open source library (BifacialSimu [12]) can be used without further programming knowledge with a graphical user interface, so that knowledge about energy yield simulations of bifacial PV systems is made accessible.

The bifacial PV module's performance is then calculated by applying a one-diode model, using the simulation radiance data for the front and rear sides of the module. Because there are no existing datasets about the albedo of red soil or soil in Ghana, measurements were carried out at three different locations in Ghana in February 2020.

The albedo is measured using two pyranometers with Class A standard, offsetting at 180° [13]. It is defined as the ratio of reflected irradiance from the ground surface to the incident radiation received upon it. One pyranometer faces up to measure the global irradiance, and the other faces down to measure the reflected irradiance from the ground.

The albedo measurement method follows the ASTM standard testing method E1918 [14]. This method allows the calculation of reflectance based on incoming radiation, but from only one pyranometer. In this case, a dual pyranometer is used to perform the solar reflectance study. Clear-sky weather conditions and a zenith angle to the test surface of less than 45° are required. For all albedo measurements, a combined standard uncertainty is calculated and considered during the discussion, following DIN EN 12975 [15]. The t-distribution is applied to determine the degrees of freedom for the uncertainty [16]. The bifacial yield simulation is carried out using the average albedo of red soil from the conducted measurements.

The empirical evidence (i.e., measurements) is analysed quantitatively. The conclusion is built qualitatively, by evaluating the study's outcomes and comparing them with a quantitative literature review. The albedo measurement setup is described in the following paragraph.

3. Albedo Measurements

The albedo is measured using an albedometer composed of two pyranometers (Class A) of the same type, offsetting at 180°. The Class A standard is the highest of the pyranometer classes. Notably, the maximum daily uncertainty of the measured albedo value is given at 2% [17].

The reflectiveness of the surroundings and the measurement setup impact the precision of the albedo measurements. The mounting system is nonreflective, and to avoid self-shading effects, the pedestal is extended toward the equator. When the pyranometer is positioned at a distance of 1 m above the soil, the fraction of light reflected from the pyranometer to the soil and back to the sensor is negligible.

All irradiance incidence in the area shadowed by the albedometer is assumed to be atmospheric hemispherical diffuse radiation [18]. The radiation on the downward-facing pyranometer combines the reflected radiance from the shaded and unshaded segments of the area. Consequently, the scattered radiation from the pyranometer to the shadowed area on the ground is part of the sky radiation.

3.1. Albedo Measurement Setup

Three measurement campaigns were performed in Ghana, in the cities of Accra, Akwatia and Kumasi. Ideally, the measurement area should be surrounded by a soil of the same kind to minimize measurement uncertainty caused by the reflection of another surface [18]. The physical characteristics of the three soil samples were analysed and showed similar compositions of quartz, kaolinite and goethite. In terms of the red colour, the samples have a +/−4% difference. The surroundings contained the same type of soil, with comparable roughness to the sample area, for all three measurements. There were no visible differences in the condition or moisture of the soil. The measurement setup is shown in Figure 1.

Figure 1. Setup of albedo measurement in Akwatia, Ghana, on the 6 February 2020. The measurement area was cleared of bigger stones and objects, and the albedometer was placed in the middle of the 2×2 m square.

The clearance of the surroundings has an impact on the albedo measurement. The measurement area was cleared so that no distractions would interfere with the albedo measurements of the red soil. The measurement data were recorded with a data logger recording two analogue radiance signals, one from the pyranometer facing the soil and one for the corresponding global irradiation. The analogue inputs are configured with a 24-bit resolution and deliver the pyranometer signal (U_{Signal}) in [μV]. They are used with a bipolar input, which offers a sensitivity value of the logging system ($W_{Sensitivity}$) in [μV/W/m^2]. The output signal is converted into the solar irradiance value (E_{Solar}) in [W/m^2] by dividing by $W_{Sensitivity}$ [17]. The measurement interval is set to 1 s; the logging interval is set to 5 s. The response time of the pyranometers is stated to be less than 5 s [17]. With the derived data, the albedo (α) is calculated following Equation (1), by dividing the reflected hemispherical radiance ($E_{Solar-up}$) by the incoming hemispherical irradiance (E_{Solar_down}):

$$\alpha = \frac{E_{Solar-up}}{E_{Solar-down}} \tag{1}$$

The average albedo is calculated for every measurement location considering the whole measurement period. The average albedo of all three locations is used to apply an empirical resolved albedo model for the bifacial yield simulation. The three different soil samples were analysed for their mineralogy, particle size and chemical composition.

3.2. Field Measurements

Three different locations in Ghana are considered. The measurement procedure and time period were similar; only the starting times varied due to the occurrence of clouds.

3.2.1. Accra

The measurement in Accra was performed on the grounds of the William Galloway Library. Before starting the measurement, the first layer of surface soil was blended to remove any stones which do not belong to the red soil, such as concrete. Additionally, all plastic waste in the measurement area was removed to prevent unwanted reflections. The measurements were performed between 12:09 P.M. and 2:09 P.M. on 11 February 2020. During the whole measurement period, no clouds were present. Therefore, no separate investigation of interrupted time periods needed to be conducted. The average albedo calculated over the 2-h measurement period was 0.269.

3.2.2. Akwatia

The measurement in Akwatia was performed on the grounds of the Akwatia St. Dominic Primary and Junior High School. It was carried out between 11:16 A.M. and 1:16 P.M. on 6 February 2020, when the sun was in zenith position. The measurement period was predominantly cloudless, and no external shadows were cast on the measurement surface. The average albedo over red soil in Akwatia was 0.200. This value was determined over two hours. Two fully cloudless periods were investigated separately (12:06 P.M.–12:16 P.M. and 12:55 P.M.–1:02 P.M.) to avoid possible measurement errors due to clouds. During the cloudless times, the albedo was 0.205, which shows a deviation of 2.6% from the albedo measured over the whole measurement period, and is therefore considered consistent.

3.2.3. Kumasi

The albedo measurement was performed at the Technical University of Kumasi between 12:30 P.M. and 2:30 P.M. The first ground layer was blended to remove unwanted particles. No clouds were present during the whole measurement period; therefore, no separate investigation of specific time periods was conducted. The average albedo over the 2-h measurement in Kumasi was 0.310.

3.3. Albedo Measurement Uncertainty

For all albedo measurements, the occurring uncertainties ($\Delta \alpha$) are considered systematic errors. All uncertainties are estimated with a Gaussian distribution; therefore, 68% of the individual measurements are between α-$\Delta \alpha$ and α+$\Delta \alpha$. A combined standard uncertainty is calculated for all measured albedo values and considered for the simulation [19]. For the calibration of the reference pyranometer, the calibration facilitator, German Aerospace Center (DLR), assumes a possible error of 1.92%. The pyranometers were calibrated four weeks before the measurement; therefore, the calibration deviation over time is negligible. Due to imperfections in the glass domes and angular reflection properties, pyranometers have a directional error. It is defined as the sum of the azimuth and zenith errors. Kipp and Zonen specify the maximal relative zenith response error in any azimuth direction, which equals the combination of the azimuth and zenith error of a horizontally mounted pyranometer as a function of the zenith angle [17]. To minimize this error, the glass domes were cleaned before each measurement. Nevertheless, the directional error is estimated at $\pm 0.2\%$, considering a maximum radiance of 1000 W/m^2. It is assumed to be the same for both pyranometers.

Up to a temperature of 50 °C, the accuracy of the pyranometer CMP11 depends on temperature range with a maximum error of $\pm 1\%$. Because the sensitivity range is not dependent on the radiance, it is assumed to be constant for both pyranometers. For converting analogue to digital signals in the data logging system, an error of 0.05% is assumed [20]. This corresponds to the pyranometers' maximum voltage of 6 mV. For the albedo measurement and calibration, two cables of 10 m each were used. Therefore, no

additional calibration error for the cable is applied. A sensitivity error of 0.02% is assumed for each cable [17]. The overall uncertainty for hourly and daily meteorological data values is kept within 2%. Therefore, the overall significance level (α_error) is 2%.

3.4. Albedo Measurement Results

The albedo measurement results of red soil during a two-hour measurement period in three different locations in Ghana are displayed in Figure 2.
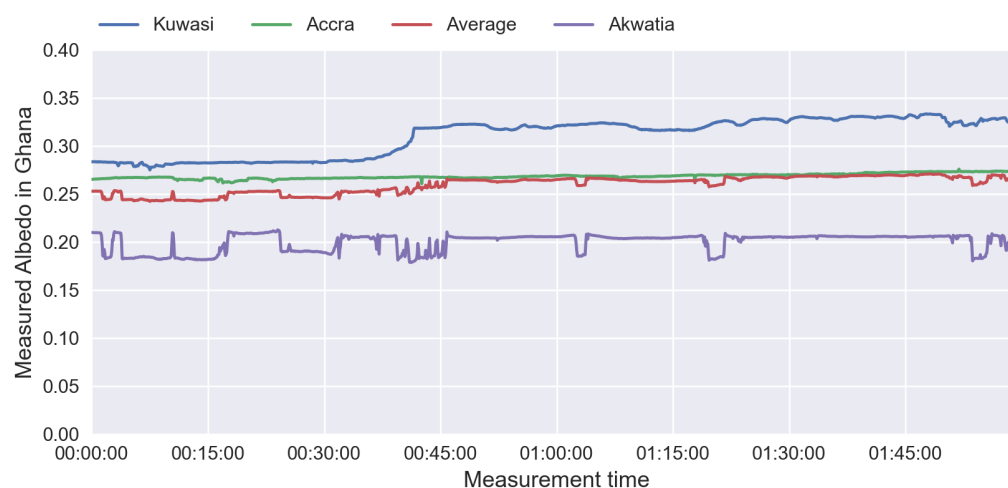

Figure 2. Albedo measurements of red soil were taken in three different locations in Ghana over a measurement period of two hours. The albedo value found in the location Kumasi is displayed in blue, Accra is displayed in green, and Akwatia is displayed in purple. The average over all three locations over the whole measurement period is displayed in red.

It can be seen that the overall albedo value in Kumasi is the highest, followed by Accra and Akwatia. The average albedo of the three named values is 0.259; this value is the input for the simulations with red soil presented in this paper. The measurements from Kumasi and Akwatia, in particular, show that the albedo fluctuates over time. This fluctuation cannot be linked to changes in cloudiness. A study on the effect of solar radiation intensity on albedo proposes that a reason could be changes in the high reflected radiation, which occurs with high incident radiation [21]. Because the albedo is measured in three different locations, the uncertainties are calculated separately, and as a combining factor, the uncertainty for the average is calculated. Due to the double-sided error interval, the degrees of freedom for the uncertainty calculation are 2.326, and consequently, the expanded uncertainty into positive and negative directions can be derived [15]. Considering error propagation, both uncertainties are considered relative error and summed up to give the total uncertainty $\Delta\alpha$ for the albedo calculation. Thus, the overall relative error is 4.86% for the top pyranometer and 4.88% for the bottom pyranometer. Only the known uncertainties described above are considered. The overall uncertainty $\Delta\alpha$ is 0.025; hence, the average albedo of red soil over the three measurements performed is $\alpha = 0.256 \pm 0.025$.

4. Front and Rear Irradiance Simulation

The power generated on the rear side of the PV module is calculated using the corresponding view factor for each shaded or unshaded area, respectively [22]. The view factor between two areas describes the fraction of the space surrounding and seen from the first area and occupied by the second area [23]. The hybrid Perez model is used as a sky model. It implies that diffuse light can be broken down into circumsolar, isotropic and horizon components [24]. Hence, a PV row is supposed to be influenced by the two rows surrounding it. The output parameters of this model are the total incident irradiance and the total absorbed irradiance on the front and rear sides of the PV array in [W/m^2].

4.1. Discretization of the Pv Array

To investigate the inhomogeneity of the irradiance on the backside of the modules, the PV array is discretized into five different segments. By applying the discretization, the radiance is calculated separately for every segment and can be summed up to get the total irradiance per row. Using this method, the differentiating irradiance distribution is taken into consideration. All values are calculated to be area-dependent in [W/m^2].

4.2. Optical Losses

The model uses a fixed angle, so that an isotropic irradiance is applied. Here, the losses for direct, circumsolar and horizon irradiance components are considered, as well as the reflection losses for isotropic reflection. Three rows are simulated with a ground coverage ratio of 0.55, at a height of 2.95 m and a tilt angle of 35°. The angle is selected due to the lower soiling rate [25]. The model makes a distinction between the total incident irradiance on a surface and the total absorbed irradiance, accounting for the angle of incidence (AOI) reflection losses. It is assumed that all losses are diffuse and therefore do not depend on the AOI.

4.3. Radiance Distribution

The view factor between every segment is calculated using the mathematical Perez model [24] for reflections and the 2D view factor model [11] for radiation. In this way, the outgoing irradiance of every segment and every PV row is calculated. The view factor from surface A_1 to surface A_2 "represents the fraction of the space surrounding and seen by" [11] surface A_1 and occupied by surface A_2. View factors are usually used in thermal radiation heat transfer theory [26], but in this case, they are translated into a general irradiance simulation.

The equilibrium of reflections between all segments of the PV array surfaces is accounted to calculate the incoming irradiance. Additionally, every segment is divided into two coordinates for every timestamp. Systematic analytical solutions are used, instead of numerical integration of double integral solutions, to speed up the calculation.

For each segment (i), the outgoing radiative flux ($q_{0,1}$) from the assigned segment is calculated using the sum of the emitted radiative flux from a segment ($q_{qemitted,i}$) and the reflected flux from a segment i ($q_{reflected,i}$) by applying Equation (2).

$$q_{0,1} = q_{emitted,i} + q_{reflected,i} \left[\frac{W}{m^2} \right] \tag{2}$$

The outgoing radiative flux ($q_{0,i}$) is assumed to be negligible in the following part. The operating temperatures are under 330 K and therefore can be associated with the emission of lower energy photons than the photons in the visible spectrum reflected by the surfaces. For this reason, a more straightforward linear system is applied to determine the outgoing radiative flux (q_0), the reflected irradiance in the form of the spectral radiosity matrix (R) [26], the view factor (F) [24] and the sky irradiance term (*Sky* as shown in Equation (3).

$$q_0 = R \cdot (F.q_0 + Sky)$$
$$Sky = (R^{-1} - F).q_0 \tag{3}$$

The resulting view factor matrix for an annual simulation has the shape [number of segments + 1, number of segments + 1, 8760] as an hourly calculation. The first two dimensions need to have one segment more than the number of segments of the PV module because the sky is considered an additional segment. The last dimension can be explained by the simulation's length and data resolution. In this case, one year equals 8760 h.

Assuming a linear current response of the bifacial module for the inhomogeneous illumination on the rear side, the electrical performance can be calculated using a one-diode equivalent model [27].

5. Energy Yield Calculation

The electrical output is calculated using the one-diode model. The direct and diffuse light is allocated differently on the rear side compared with the front side, on which the direct light is more reflected onto the bottom of the bifacial PV module.

There are different approaches to evaluating a bifacial PV module's front and rear parameters. This study takes the values measured simultaneously on both sides with two light sources, as indicated in the module datasheet. According to a 12-month study on a PV lighthouse [27], the annual mismatch losses are around 0.23% and therefore can be discounted in the simulation.

The following approach converts monofacial indoor measurements on both sides of the bifacial PV module to bifacial outdoor conditions [28]. The calculated front and rear side irradiance ($qabs$) is used to calculate the total current (I_{sc-bi}) and voltage (V_{oc-bi}) of the bifacial module by multiplying the front side current (I_{sc-f}) with the ratio of the front side irradiance ($qabs_{front}$) and the irradiance at Standard Test Conditions (STC) (G_{f0}). The same ratio is calculated for the rear side irradiation ($qabs_{rear}$) with the rear irradiance at STC (G_{r0}) and the rear side short circuit current (I_{sc-r}), as shown in Equation (4). The module current is calculated as the sum of the front and rear currents, due to the assumption of a linear current response under different light intensities. The front and rear open-circuit current, voltage and fill factor are multiplied with the aligning temperature coefficient between the current and ambient temperatures to take the current temperature into account.

$$I_{sc-bi} = \frac{qabs_{front}}{G_{f0}} \cdot I_{sc-f} + \frac{qabs_{rear}}{G_{r0}} \cdot I_{sc-r} \tag{4}$$

The gain in short-circuit current (R_{Isc}) is calculated by accounting for the relation of the bifacial short-circuit current (I_{sc-bi}) with the front short-circuit current (I_{sc-f}), as displayed in Equation (5).

$$R_{isc} = \frac{I_{sc-bi}}{I_{sc-f}} = \frac{qabs_{front}}{G_{f0}} + \frac{qabs_{rear}}{G_{r0}} \cdot \frac{I_{sc-r}}{I_{sc-f}} \tag{5}$$

Following the open circuit terms [28] in an ideal one-diode model, the bifacial open-circuit voltage (V_{oc-bi}) is calculated using the open-circuit voltage for the front (V_{oc-f}) and the rear side (V_{oc-r}) in Equation (6).

$$V_{oc-bi} = V_{oc-f} + \frac{(V_{oc-r} - V_{oc-f}) \cdot \ln(R_i sc)}{\ln(\frac{I_{sc-r}}{I_{sc-f}})} \tag{6}$$

Considering the model of Singh et al. [27], the bifacial fill factor (FF_{bi}) is calculated with the pseudo fill factor (pFF), the fill factor at STC for the front (FF_{f0}) and rear side (FF_{r0}), the short circuit current at STC for the front (I_{sc-f0}) and the rear side (I_{sc-r0}), as displayed in Equation (7).

$$pFF = \frac{\frac{I_{sc-r0}}{I_{sc-f0}} \cdot FF_{f0} - FF_{r0} \cdot \frac{V_{oc-r0}}{V_{oc-f0}}}{\frac{I_{sc-r0}}{I_{sc-f0}} - \frac{V_{oc-r0}}{V_{oc-f0}}} \tag{7}$$

The yearly energy yield (E_{bi}) of the bifacial system in [kWh/m^2] is calculated for every hour of the investigated time period and summed up with Equation (8).

$$E_{bi} = FF_{bi} \cdot V_{oc-bi} \cdot I_{sc-bi} \tag{8}$$

The computed power density for a timestamp is given as an area-dependent value in kW/m^2, and then the values are integrated to calculate the annual energy yield. Hereafter, the occurring measurement uncertainties are described.

6. Impact Analysis

Applying the front and rear radiance simulation described and the energy yield calculation, the energy yield for a bifacial system with three rows, consisting of the modules GCL-M3/72 GDF with 420 Wp each and an efficiency of 19.8%, in northern Ghana with an average global horizontal irradiance of 2162 kWh/m^2 per year is calculated. The system has a height of 2.95 m and faces southeast with a ground coverage ratio of 55%. For this scenario, the yearly bifacial output energy per module area is 508.8 kWh/m^2. In comparison, the yearly monofacial output energy per module area is 430.2 kWh/m^2, which results in a bifacial gain of 18.3%. The simulated location is Tamale in northern Ghana, which has an average global horizontal irradiance of 2162.4 kWh/m^2.

6.1. Impact on Energy Yield

The basis of the energy yield calculation is the bifacial radiance simulation, based on the view factors. The summary of the simulation results show that the total incident irradiance on a surface, the sum of the front and rear sides of the bifacial PV modules, strongly depends on the applied albedo. For a lower uncertainty level with an albedo of 0.235, the yearly bifacial gain is 17.1%, while for the higher uncertainty level, it is 19.4%. This leads to a deviation in the energy yield of −6.3% by underestimating the albedo and +6.3% by overestimating the albedo.

Figure 3 displays the total incident irradiance on the module surface [W/m^2] over the year, considering the average of three simulated rows. The irradiance on the front side is in blue, and the irradiance on the rear side is displayed in orange. It can be seen that the sum of average front and rear side irradiance reaches values of more than 800 W/m^2.
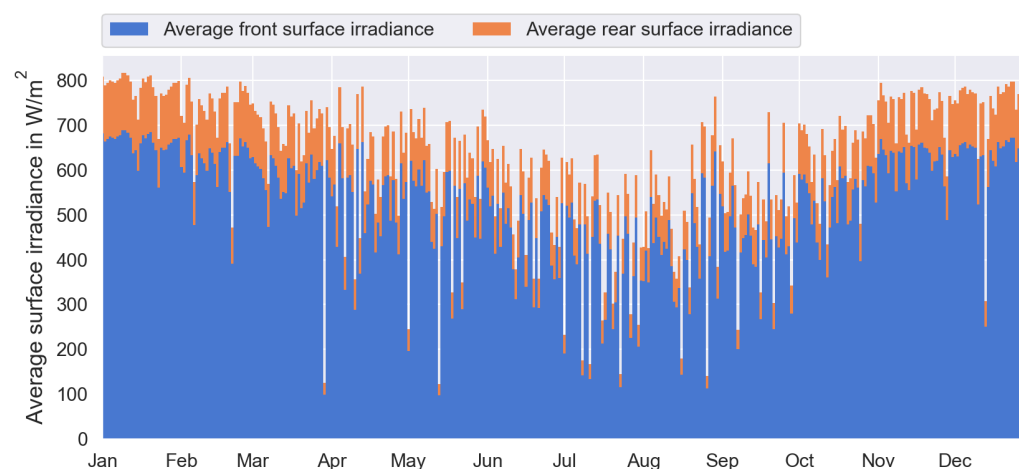

Figure 3. Simulated average front and rear irradiance over one year for the average of the three rows. The average front surface irradiance is displayed in blue. The average rear surface irradiance is displayed in orange.

Figure 4 displays the consideration of three rows individually, with an average albedo. It is noticeable that the first row is reached by the highest amount of irradiance, followed by the second and the third row. This effect is justified by row shading effects from the rows in front of the one considered.
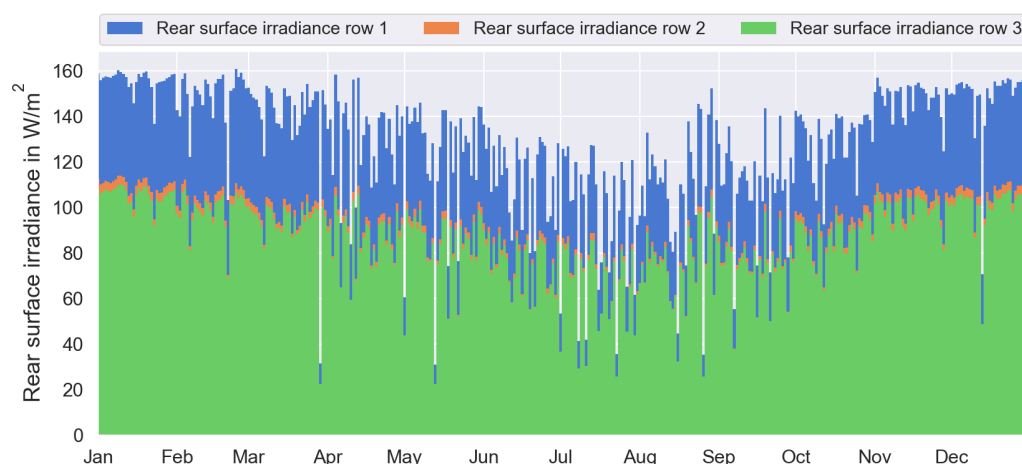
Figure 4. Simulated average rear irradiance over one year, differentiated for three rows. Row 1 is displayed in blue, Row 2 in orange and Row 3 in green. The highest variance can be seen in Row 1.

6.2. Comparison of Average and Resolved Albedo

The presented values are calculated using an average of the conducted albedo measurements. Under outdoor conditions, the surface's diurnal albedo behaves asymmetrically, as displayed in Figure 5.
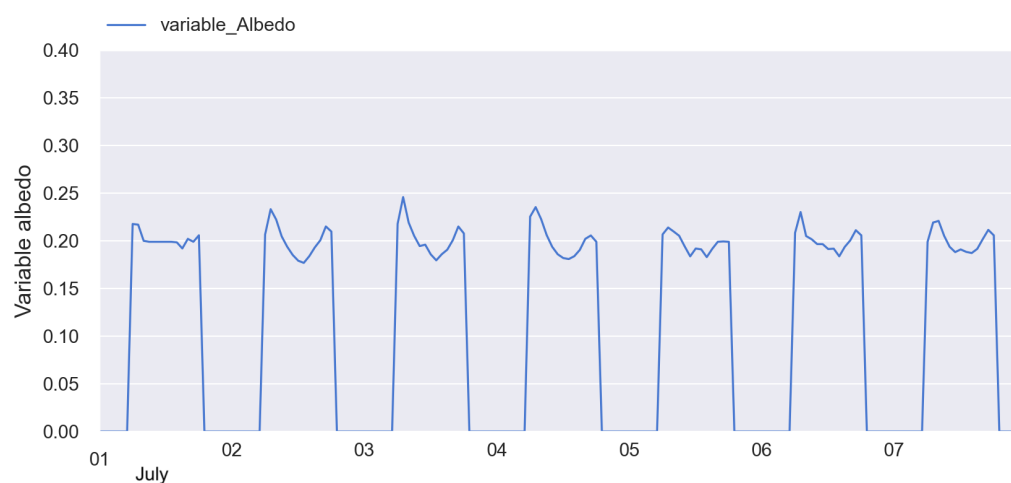
Figure 5. Simulated diurnal average albedo over the first week of July 2020 in Ghana. A typical curve for a variable albedo can be observed, with higher values in the morning and evening compared with midday.

The higher albedo values in the morning and afternoon than around noon indicate that the albedo is dependent on the solar zenith angle [29]. This relation has been stated to be exponential [30]. Several measurements have reported lower values in the mornings than in the afternoons, and vice versa [31].

Applying a simple resolved albedo model, the energy yield simulation results in a bifacial gain of 15.4% with a mean albedo of 0.2, which equals 20%. Therefore, the lower mean albedo leads to a deviation of -15.7% for the bifacial gain. However, the spectral dependence of the albedo that occurs in reality is not taken into account in this study, due to the unavailability of spectral reflectivity measurements. The course of the spectral albedo is influenced by the ratio of direct and diffuse irradiance. The height of the modelled spectral albedo is affected by the reflectivity spectrum and will be considered in future studies. A spectral albedo model is already integrated in the open-source simulation program BifacialSimu [12].

7. Discussion and Conclusions

Obtaining the exact surface albedo for bifacial solar energy simulations is considered an essential task due to the high impact of the albedo on the energy yield.

Three measurements of the albedo of red soil in Ghana were carried out. The albedo measurements ranged from 0.200 to 0.310. Considering measurement uncertainty, the albedo range of the red soil from the three measurements was between 0.175 and 0.335. The calculated average albedo of red soil in Ghana is 0.260 ± 0.025.

Considering the average albedo for red soil on a bifacial PV system in northern Ghana, the yearly energy yield is 508.8 kWh/m^2, with a bifacial gain of 18.3%. With the application of an underestimated or overestimated albedo, the energy yield has a deviation of -6.3% or +6.3%, respectively. The primary outcome of this study is that the albedo of red soil varies in different locations and must always be measured on site for exact simulation. Red soil is generally considered a suitable surface for bifacial PV systems due to its albedo. No correlation could be found between the albedo and mentioned geological properties. However, compared with darker soils, red soil has a positive impact on the energy yield of bifacial PV systems.

More studies should be directed toward the impact of red dust accumulation on the performance of bifacial PV modules in Western Africa, because the sector is growing significantly [32]. A detailed investigation of the impacts of different soils, considering their physical characteristics, is required to analyse the impact on bifacial PV module performance. This paper uses a unique dataset as fundamental research regarding red soil in sub-Saharan Africa. Because the deposition of red soil on PV modules, compared with other dust components, leads to worse results, the investigation of soil with this colour and its influence on the performance of bifacial PV modules is essential.

Author Contributions: E.-M.G. designed the software and the computational framework and carried out the investigation in Ghana. U.B. supervised the study and was in charge of the overall project administration. E.-M.G. wrote the manuscript with input from all authors. J.-R.H.-M. reviewed the manuscript. All authors have read and agreed to the published version of the manuscript.

Conflicts of Interest: The authors declare no conflict of interest.

Abbreviations

The following abbreviations are used in this manuscript:

α	Albedo of a surface.
E_{bi}	Yearly energy yield.
E_{solar}	Solar irradiance.
F	View factor.
FF	Fill factor.
G	Irradiance at Standard Test Conditions.
I_{sc}	Front side current.
pFF	Pseudo fill factor.
R	Spectral radiosity matrix.
R_{isc}	Short-circuit current gain.
q	Radiative flux.
$qabs$	Rear side irradiance.

References

1. Grommes, E.M.; Blieske, U.; Hadji-Minaglou, J.R. Positive Impact of Red Soil on Albedo and the Annual Yield of Bifacial Photovoltaic-Systems in Ghana. In Proceedings of the 17th Conference on Sustainable Development of Energy, Water and Environment Systems (SDEWES), Paphos, Cyprus, 6–10 November 2022.
2. Petrova-Koch, V.; Hezel, R.; Goetzberger, A.; Rhodes, W.T.; Adibi, A.; Asakura, T.; Hänsch, T.W.; Kamiya, T.; Krausz, F.; Monemar, B.; et al. (Eds.) *High-Efficient Low-Cost Photovoltaics: Recent Developments*; Springer Series in Optical Sciences; Springer: Berlin/Heidelberg, Germany, 2009; Volume 140. [CrossRef]
3. International Technology Roadmap for Photovoltaic (ITRPV). 2022 Results. 2022. Available online: https://www.vdma.org/international-technology-roadmap-photovoltaic (accessed on 16 February 2023).
4. Hall, M. South Africa's First Solar Wheeling Project. *PV Mag.* **2021**. Available online: https://www.pv-magazine.com/2021/11/08/south-africas-first-solar-wheeling-project/ (accessed on 16 February 2023).
5. Suri, M.; Cebecauer, T.; Meyer, A.J.; Van Niekerk, J.L. Accuracy—Enhanced Solar Resource Maps of South Africa. 2015. Available online: https://solargis2-web-assets.s3.eu-west-1.amazonaws.com/public/publication/2015/19db7a4fa7/Suri-et-al-SASES2015-Accuracy-enhanced-solar-resource-maps-of-South-Africa.pdf (accessed on 16 February 2023).
6. Dewitte, O.; Jones, A.; Spaargaren, O.; Breuning-Madsen, H.; Brossard, M.; Dampha, A.; Deckers, J.; Gallali, T.; Hallett, S.; Jones, R.; et al. Harmonisation of the Soil Map of Africa at the Continental Scale. *Geoderma* **2013**, *211–212*, 138–153. [CrossRef]
7. Asumadu-Sarkodie, S.; Owusu, P.A. The Potential and Economic Viability of Solar Photovoltaic Power in Ghana. *Energy Sources Part Recover. Util. Environ. Eff.* **2016**, *38*, 709–716. [CrossRef]
8. Grommes, E.M.; Mebus, S.; Ray, C.B.; Depner, K.; Pillai, A.; Blieske, U. Comparison of the Yield of Miniaturized Bifacial Photovoltaic Modules with the Yield Simulation of Bifiacial Modules. In Proceedings of the 8th World Conference on Photovoltaic Energy Conversion, Milan, Italy, 26–30 September 2022; pp. 772–776. [CrossRef]
9. Grommes, E.M.; Nows, S.; Klag, F.; Schemann, F.; Blieske, U. Simulation of the Irradiance and Yield Calculation of Bifacial PV Systems in the USA and Germany by Combining Ray Tracing and View Factor Model. In Proceedings of the 8th World Conference on Photovoltaic Energy Conversion, Milan, Italy, 26–30 September 2022; pp. 1004–1008. [CrossRef]
10. Ineichen, P.; Guisan, O.; Perez, R. Ground-Reflected Radiation and Albedo. *Sol. Energy* **1990**, *44*, 207–214. [CrossRef]
11. Anoma, M.A.; Jacob, D.; Bourne, B.C.; Scholl, J.A.; Riley, D.M.; Hansen, C.W. View Factor Model and Validation for Bifacial PV and Diffuse Shade on Single-Axis Trackers. In Proceedings of the 2017 IEEE 44th Photovoltaic Specialist Conference (PVSC), Washington, DC, USA, 25–30 June 2017; pp. 1549–1554. [CrossRef]
12. Grommes, E.M.; Blieske, U. BifacialSimu: Holistic Simulation of Large-Scale Bifacial Photovoltaic Systems. *J. Open Source Softw.* **2022**, *7*, 4443. [CrossRef]
13. *ISO 9060:2018*; Solar Energy—Specification and Classification of Instruments for Measuring Hemispherical Solar and Direct Solar Radiation. ISO: Geneva, Switzerland, 2018.
14. Akbari, H.; Levinson, R.; Berdahl, P. ASTM Standards for Measuring Solar Reflectance and Infrared Emittance of Construction Materials and Vomparing Their Steady-State Surface Temperatures. *Present. Am. Counc. Energy Effic. Econ. Summer Study* **1996**, *1*, 1–9.
15. Grommes, E.M.; Blieske, U.; Müller-Ost, J. The Impact of Albedo Measurements on Power Density Calculations of Bifacial Modules. In Proceedings of the 37th European Photovoltaic Solar Energy Conference and Exhibition, Online, 7–11 September 2020; pp. 1228–1232. [CrossRef]
16. Student. The Probable Error of a Mean. *Biometrika* **1908**, *6*, 1–25. [CrossRef]
17. Kipp & Zonen B.V. *Instruction Manual: CMP Series Pyranometer*; Technical report; Kipp&Zonen B.V.: Delft, The Netherlands, 2016.
18. Matthias, A.D.; Post, D.F.; Accioly, L.; Fimbres, A.; Sano, E.E.; Batchily, A.K. Measurement of Albedos for Small Areas of Soil. *Soil Sci.* **1999**, *164*, 293–301. [CrossRef]
19. *Solar Collectors—General Requirements*; Technical report; Beuth Verlag GmbH: Berlin, Germany, 2018; p. 12975. [CrossRef]
20. Kipp & Zonen B.V. *Instruction Manual Logbox SE: V2020-06*; Technical report; Kipp&Zonen B.V.: Delft, The Netherlands, 2020.
21. Chen, J.; Zhou, Z.; Wu, J.; Hou, S.; Liu, M. Field and Laboratory Measurement of Albedo and Heat Transfer for Pavement Materials. *Constr. Build. Mater.* **2019**, *202*, 46–57. [CrossRef]
22. Grommes, E.M.; Blieske, U.; Müller-Ost, J. Performance Estimation of Bifacial PV Systems Using the View Factor Matrix. In Proceedings of the 15th Conference on Sustainable Development of Energy, Water and Environment Systems, Cologne, Germany, 1–5 September 2022. [CrossRef]
23. Meseguer, J.; Pérez-Grande, I.; Sanz-Andrés, A. 5—Thermal Radiation Heat Transfer. In *Spacecraft Thermal Control*; Meseguer, J., Pérez-Grande, I., Sanz-Andrés, A., Eds.; Woodhead Publishing: Sawston, UK, 2012; pp. 73–86. [CrossRef]
24. Perez, R.; Seals, R.; Ineichen, P.; Stewart, R.; Menicucci, D. A New Simplified Version of the Perez Diffuse Irradiance Model for Tilted Surfaces. *Sol. Energy* **1987**, *39*, 221–231. [CrossRef]
25. Cano, J.; John, J.J.; Tatapudi, S.; Tamizhmani, G. Effect of Tilt Angle on Soiling of Photovoltaic Modules. In Proceedings of the 2014 IEEE 40th Photovoltaic Specialist Conference, PVSC 2014, Denver, CO, USA, 8–13 June 2014; pp. 3174–3176. [CrossRef]
26. Gross, U.; Spindler, K.; Hahne, E. Shapefactor-Equations for Radiation Heat Transfer between Plane Rectangular Surfaces of Arbitrary Position and Size with Parallel Boundaries. *Lett. Heat Mass Transf.* **1981**, *8*, 219–227. [CrossRef]
27. Singh, J.P.; Aberle, A.G.; Walsh, T.M. Electrical Characterization Method for Bifacial Photovoltaic Modules. *Sol. Energy Mater. Sol. Cells* **2014**, *127*, 136–142. [CrossRef]

28. Janssen, G.J.M.; Van Aken, B.B.; Carr, A.J.; Mewe, A.A. Outdoor Performance of Bifacial Modules by Measurements and Modelling. *Energy Procedia* **2015**, *77*, 364–373. [CrossRef]

29. Yue, X.; Li, Z.; Zhao, J.; Fan, J.; Takeuchi, N.; Wang, L. Variation in Albedo and Its Relationship With Surface Dust at Urumqi Glacier No. 1 in Tien Shan, China. *Front. Earth Sci.* **2020**, *8*, 110. [CrossRef]

30. Nkemdirim, L.C. A Note on the Albedo of Surfaces. *J. Appl. Meteorol. Climatol.* **1972**, *11*, 867–874. [CrossRef]

31. Ziar, H.; Sönmez, F.F.; Isabella, O.; Zeman, M. A Comprehensive Albedo Model for Solar Energy Applications: Geometric Spectral Albedo. *Appl. Energy* **2019**, *255*. [CrossRef]

32. Menoufi, K. Dust Accumulation on the Surface of Photovoltaic Panels: Introducing the Photovoltaic Soiling Index (PVSI). *Sustainability* **2017**, *9*, 963. [CrossRef]